ELECTRON CYCLOTRON RESONANCE HEATING IN THE CURRENT RAMP-UP PHASE OF TEXTOR-94

E. Westerhof[1)], C.J. Barth[1)], A.J.H. Donné[1)], J.A. Hoekzema[2)], G.M.D. Hogeweij[1)], R.J.E. Jaspers[1)], H.R. Koslowski[2)], A. Krämer-Flecken[2)], N.J. Lopes Cardozo[1)], H.J. van der Meiden[1)], T. Oyevaar[1)], F.C. Schüller[1)], V.S. Udintsev[1)], and TEC Team

Partners in the Trilateral Euregio Cluster (TEC)
1) FOM-Instituut voor Plasmafysica "Rijnhuizen", Association EURATOM-FOM, Postbus 1207, NL-3430 BE Nieuwegein, Netherlands

2) Institut für Plasmaphysik, Forschungszentrum Jülich GmbH, EURATOM Association, D-52425 Jülich, Germany

I. Introduction

Experiments with electron cyclotron resonance heating (ECRH) on TEXTOR-94 [1] have confirmed some of the striking results obtained in RTP [2,3]: self-organised structures in the form of high temperature filaments [4] and the existence of very localised electron transport barriers near surfaces with rational values of the safety factor q. These results suggest a direct relation between electron heat conductivity and the local value of q, with low values of the heat conductivity in narrow regions near rational values of q [3]. Such a relation between the heat conductivity and q, could well be exploited to create scenarios with optimised q-profiles, creating wide transport barriers in regions of low or inverse shear. Such profiles occur naturally during the current ramp-up phase of a discharge, in particular, when current penetration is delayed by early additional heating. This has motivated the experiments on ECRH in the current ramp-up phase of TEXTOR-94, which are reported here.

II. Experimental Scenario

A standard plasma start-up scenario for TEXTOR-94 is used in which a fast (100 ms) current initialisation (up to $I_p(0.1\ s) \approx 200$ kA) is followed by a 500 ms controlled current rise of 0.3 MA/s up to the full plasma current of $I_p = 350$ kA. Early additional heating is applied starting from t = 0.2 s by counter-neutral beam injection (NBI). This serves the purpose of both stabilising the discharge by differential rotation [5] as well as extending the phase with possible negative central shear (NCS) and delaying the onset of sawteeth. In case of counter-NBI, the latter is further aided by a central counter-driven current. A small amount of co-NBI is applied for diagnostic purposes: Charge exchange recombination spectroscopy, CXRS, for T_i and rotation velocity. During this phase ECRH (110 GHz, 2nd harmonic X-mode, 200 ms, 270 kW injected into the plasma) is applied, typically from t = 0.250 s to t = 0.450 s. The diamagnetic energy shows that the confinement in this phase is slightly below L-mode scaling and does not change with the application of ECRH.
High spatial resolution density n_e and temperature T_e measurements are obtained during the ECRH phase by a double pulse Thomson scattering diagnostic [6]. The temporal evolution of both n_e and T_e is available from a HCN-interferometer and an ECE-radiometer. Measurements of the poloidal magnetic field and, hence, the safety factor q are obtained by FIR-polarimetry.

III. Experimental Results

III.1. Temperature and Density Barriers, Profile Evolution

The electron temperature is measured at t = 0.35 s, midway in the ECRH pulse, for a series of discharges in which the location of the EC power deposition has been changed by varying the magnetic field from B_ϕ = 1.85 to 2.35 T. Central heating is obtained for B_ϕ = 2.00 to 2.10 T, where the shift with respect to the EC resonance, at B = 1.96 T, is due to the Shafranov shift. The data reveal the existence of two transport barriers at normalised minor radii of ρ = 0.13 and 0.35. Both barriers can be identified on individual T_e profiles, Fig. 1. Note, that the inner barrier is significantly broader than the deposition profile, which for central heating can be as narrow as $\Delta\rho$ = 0.05. The width of the ECRH deposition has been varied by varying the EC beam focus. However, even for the largest beam width, for central resonance the power deposition width did not exceed the width of the inner barrier. Under these conditions the width of the inner barrier is independent of the width of the EC deposition profile.

The inner barrier is also clearly seen on the density profile, Fig. 2. Although the density profiles with NBI-only and NBI+ECRH are indistinguishable, the NBI-only discharges show MHD activity with collapses of both n_e and T_e. Figure 2 also shows the density profile as measured in a NBI-only discharge only 3 ms after such a collapse. Here the steep density gradient at the edge of the inner barrier is even more pronounced, which demonstrates that the collapse leaves the region inside the barrier largely unaffected.

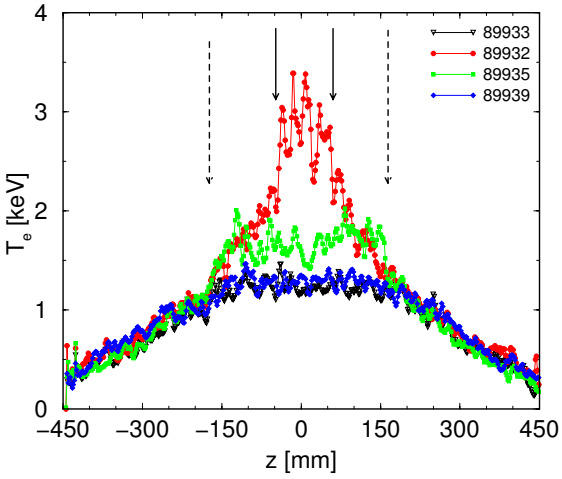

Fig.1 T_e-profiles from Thomson scattering at t = 0.350 s for three different position of ECR: #89932 $\Delta\rho_{EC}$ = 0.06; #89935 $\Delta\rho_{EC}$ = 0.23; #89939 $\Delta\rho_{EC}$ = 0.50; #89933 NBI-only.

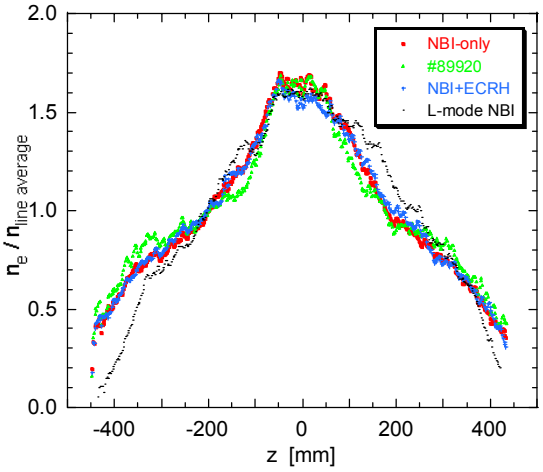

Fig.2 Normalised density profiles for discharges with NBI-only (red) and with NBI + central ECRH. The profile in the current flat top of a low density L-mode discharge is given for comparison.

Although large collapses are not observed in the discharges with NBI plus central ECRH, some minor ones are still present. The ECE data appear to show that position of the barriers also varies during the ECRH pulse, although the spatial resolution of the ECE diagnostic is insufficient for a clear identification of the barriers. Thomson scattering measurements at different times in a set of three similar discharges show that the central pressure is practically constant, and that the width of the central barrier varies only slightly. As the heating is moved off-axis, the discharge becomes more prone to MHD instabilities. This is illustrated in Fig. 3, which shows the central temperature from ECE for four different locations of the EC power deposition. Note in particular discharge #89940, where ECRH is located at the position of the inner barrier: a large collapse is observed that seems to indicate the transient loss of the inner barrier.

III.2. Current Penetration

In spite of the higher T_e, ECRH is seen to lead to a faster current penetration because of the strong peaking of the temperature profile: the onset of sawteeth is found to occur close to the end of the ECRH pulse. Calculations of the current diffusion (Fig. 4) starting from a strongly hollow current density profile at t = 0.100 s, and using the experimental T_e profiles with (neo)classical current penetration (including effects of bootstrap current and a beam driven current of about -40 kA) yield almost flat central q profiles with q close to 2 at the beginning of the ECRH pulse, down to about 1 at the end of ECRH. Within experimental uncertainties, these values are consistent with measurements of the central q value from polarimetry. Midway during ECRH $q_0 = 1.5$ is crossed near the time of the minor collapse as observed in discharge #89937 (Fig. 3). Also a shorter (88 ms) ECRH pulse is seen to prevent the large collapse as observed in NBI-only discharges, and results in the onset of sawteeth, though at the later time of t = 0.70 s. Also for NBI-only discharges both the current diffusion calculations as well as polarimetry show that q_0 drops below 1. However, in the experiments some discharges are seen to develop into sawtoothing discharges only after the switch-off of counter-NBI, while other discharges never develop sawteeth but end in a disruption already before the counter-beam is switched-off.

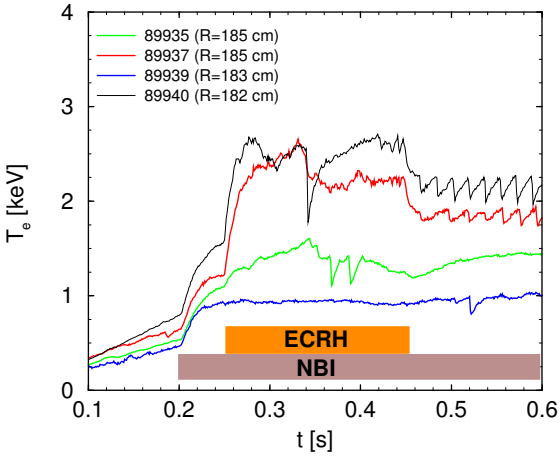

Fig.3 The evolution of $T_e(0)$ from ECE for four different positions of ECR:
#89937 $\Delta\rho_{EC} = 0.00$; #89935 $\Delta\rho_{EC} = 0.23$;
#89939 $\Delta\rho_{EC} = 0.50$; #89940 $\Delta\rho_{EC} = 0.13$.

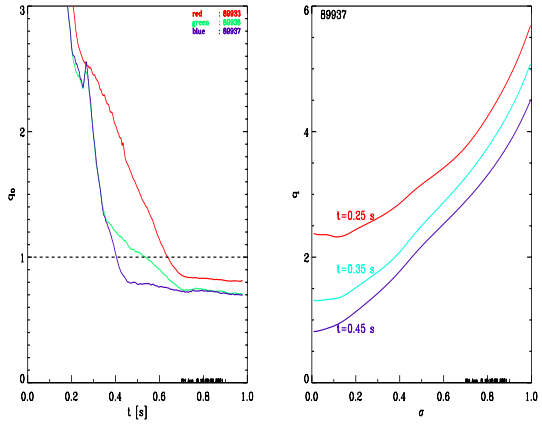

Fig.4 Evolution of q_0 from current diffusion calculations for #89937 (central ECRH), #89936 (88 ms of ECRH), and #89933 (NBI-only). Also shown are the predicted q-profiles for #89937.

III.3. Rotation Scan

In order to study the effects of rotation (and current drive) induced by the beams the balance of counter- and co-NBI has been varied keeping the total injected power constant. Relatively quiescent ECRH phases (0.250 s to 0.450 s) are only obtained with dominant counter-NBI. With central ECRH the first sawtooth occurs near or just after the end of the ECRH pulse. When the power balance is shifted by increasing co-NBI, the ECRH phase shows increasing MHD activity. In all these cases, the discharge remains unstable also after ECRH, sawteeth are never destabilised, and the discharges end in a disruption. Increasing the amount of co-NBI brings the time of the disruption forward until t ≈ 0.7 s with dominant co-NBI. The high level of MHD activity and the regular collapses appear to result in broader temperature profiles that prevent the current penetration. Discharges without pre-heating by (counter-) NBI, show large core collapses during ECRH in the current ramp phase [2].

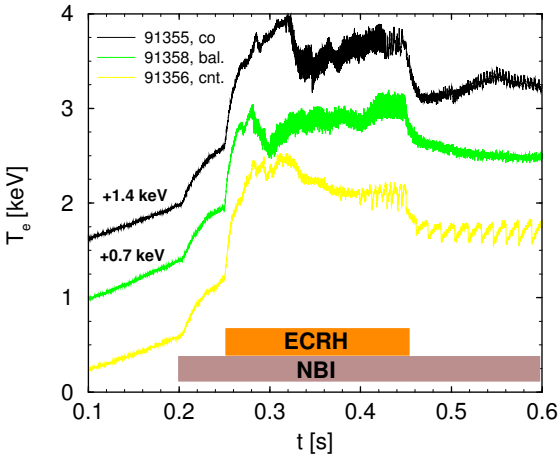

Fig.5 The evolution of $T_e(0)$ from ECE for three different ratios of co- and counter-NBI: #91355 co-NBI; #91356 counter-NBI; #91358 balanced beams.

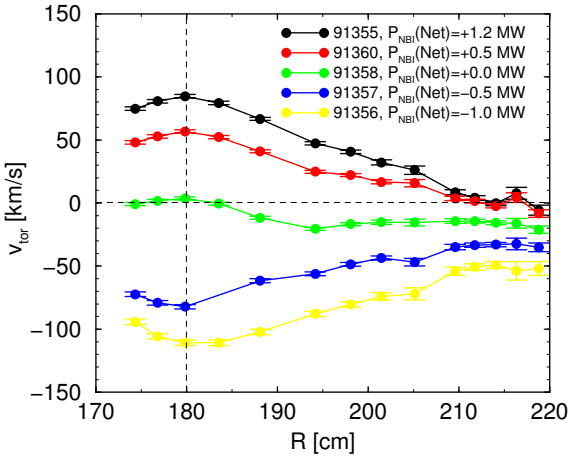

Fig.6 Profiles of rotation velocity (at t=350-400ms) from CXRS for discharges with different ratios of co- and counter-NBI. For each discharge the net power P_{co} - $P_{counter}$ is quoted.

IV. Discussion and Conclusions

ECRH during the NBI-preheated current ramp phase in TEXTOR-94 reveals the presence of multiple temperature barriers. The position of these barriers appears to be independent of the width and location of the EC power deposition. Given the strong evolution of the current density during the ECRH pulse it is difficult to identify the value of the safety factor q to which these barriers might correspond. The strong current evolution during the ECRH pulse is evident by the onset of sawteeth at the end of ECRH. The current penetration is consistent with (neo)classical current diffusion. Sawteeth are not observed in the case with NBI-only, until after the dominant counter-NBI is switched-off (provided the discharge is not terminated by a disruption earlier). Although counter-NBI in itself prevents the onset of sawteeth, it appears necessary for a MHD stable evolution of the ECR-heated current ramp. Further analysis is required to determine whether differences in wall stabilisation due to rotation or the effects of the different beam driven currents are responsible for the increased susceptibility of the discharge to MHD instabilities as the amount of co-NBI is increased.

Acknowledgements

This work was performed under the Trilateral Euregio Cluster Agreement with financial support of the Association Euratom-FOM and the Dutch research organisation NWO.

References

[1] N.J. Lopes Cardozo et al., Plasma Phys. Control. Fusion **39** (1997) B303.
[2] F.C. Schüller et al., 27th EPS Conference on Controlled Fusion and Plasma Physics, 12-16 June 2000, Budapest, Hungary.
[3] G.M.D. Hogeweij, N.J. Lopes Cardozo, M.R. de Baar, A.M.R. Schilham, Nucl. Fusion **38** (1998) 1881.
[4] A.J.H. Donné, et al., Plasma filamentation in TEXTOR-94, this conference paper P4.14.
[5] H.R. Koslowski et al., submitted for publication in PPCF, 2001.
[6] C.J. Barth, H.J. van der Meiden, T. Oyevaar and N.J. Lopes Cardozo, Rev. Sci. Instrum. **72** (2001) 1138.